Quantitative local environment characterization in amorphous oxides

Alexis Amézaga,[1,2] Erik Holmström,[3] Raquel Lizárraga,[3] Eduardo Menéndez-Proupin,[2] P. Bartolo-Pérez,[4] and Paolo Giannozzi[5,6]

[1]*Instituto de Matemáticas, Facultad de Ciencias, Universidad Austral de Chile, Casilla, Valdivia, Chile*

[2]*Departamento de Física, Facultad de Ciencias, Universidad de Chile, Las Palmeras 3425, 780-0024 Ñuñoa, Santiago, Chile*

[3]*Instituto de Física, Facultad de Ciencias, Universidad Austral de Chile, Casilla 567, Valdivia, Chile*

[4]*Departamento de Física Aplicada, CINVESTAV-IPN, Unidad Mérida, A.P. 73 Cordemex, 97310 Mérida, Yucatan, México*

[5]*Department of Physics, University of Udine, via delle Scienze 208, I-33100 Udine, Italy*

[6]*CNR-INFM DEMOCRITOS National Simulation Center, I-34014 Trieste, Italy*

(Received 13 September 2009; revised manuscript received 10 December 2009; published 27 January 2010)

We perform density-functional-theory calculations of electronic core levels to obtain the tellurium x-ray photoelectron spectra in the amorphous solar-energy materials $CdTeO_x$ (x=0.2, 1, 2, and 3). We quantify the distribution of local tellurium environments that sum up to the total two-peak structure in the experimental spectrum. The general trend is that the more oxygen neighbors tellurium has the bigger the shift of its core-level energy. However, due to the structural complexity, the relation between the core-level shift and the number of oxygen neighbors does not obey simple rules. Hence, we show the importance of computer simulations when interpreting x-ray photoelectron spectra in this system, in particular, and amorphous oxides in general.

DOI: 10.1103/PhysRevB.81.014210 PACS number(s): 79.60.Ht, 71.15.Mb, 61.43.Bn, 61.43.Dq

I. INTRODUCTION

X-ray photoelectron spectroscopy (XPS) is an element-specific probe that provides valuable information of chemical compositions, local-environment effects, and the electronic structure of solids.[1] Typically, the area under a peak in an XPS spectrum is interpreted as a measure of the relative amount of the element represented by that peak and the shape of the peak and precise position indicate its chemical state. Therefore, chemical compositions are the most straightforward information that can be obtained in the analysis of the spectrum by integrating each peak corresponding to each element.

Nevertheless, to determine different chemical environments of a single element within a material is often difficult and requires additional information to aid the analysis of the spectral line shapes, for example x-ray diffraction of the crystal structure or other knowledge that can limit the number of parameters in the curve-fitting procedure. In an amorphous material however, the absence of symmetries and infinite number of possible local environments for an element may complicate the interpretation of the experimental data.

An efficient way to analyze experimental XPS data of amorphous materials is therefore to model the amorphous structure by means of, for example, molecular dynamics (MD) and then calculate the spectrum from first principles. The advantage of this approach is that the correlation between local environments and spectral peak shapes and positions can readily be obtained since the contributions to the spectrum from individual atoms are given. Hence, the combination of calculation and experiment leads to new information that is inherently inaccessible to either one of them separately. An example of this is a study where the combination of XPS and first principles calculations was used to characterize deeply buried interfaces in metallic multilayers.[2]

The interpretation of the two tellurium peaks in amorphous CdTe oxides is an example of such a complex situation. It is clear from experiments[3–7] that the peaks are correlated with the amount of oxygen in the close chemical environment of the tellurium sites but a quantitative analysis of what particular environments that build the individual peaks is still missing.

The variations in the core-level binding energies with the atomic environment are called core-level shifts (CLS). In the present work, we calculate the tellurium CLS in a range of amorphous $CdTeO_x$ materials by means of density-functional theory (DFT).[8,9] The core-level energies are then used to compute the XPS spectra. In our calculations, we use amorphous structures that were previously calculated using *ab initio* MD simulations.[10] We investigate the correlation between the site-dependent local tellurium environments and the corresponding CLS. The calculated spectra are compared to XPS spectra of CdTe oxides films grown by rf sputtering.[3]

The paper is organized as follows: in Sec. II, we present briefly the CLS theory and the computational methods and details of the calculations. In Sec. III we discuss our results and in Sec. IV we present our conclusions.

II. THEORY

A. Core-level shifts

In the photoemission experiment the initial state consists of a crystal in its ground state plus an x-ray photon. The final state is a crystal with one electron missing in a deep core level plus an electron leaving the crystal (photoelectron). The binding energy is defined as the difference between the two states

$$E_B = E_f^{N-1} - E_i^N, \tag{1}$$

where E_i^N is the energy of the initial state with N electrons and E_f^{N-1} is the energy of the final state. The photoelectron binding energy is measured in an XPS experiment as

$$E_B = \hbar\omega - E_{\text{kin}} - \phi \tag{2}$$

where $\hbar\omega$ is the x-ray photon energy, E_{kin} is the kinetic energy of the photoelectron, and ϕ is the work function. The work function is the lowest energy an electron must overcome in order to escape from the surface and be detected. The CLS can then be defined as the difference in binding energy between atomic sites in a material and is attributed to the different local environments of the sites. For a detailed description of XPS, see Refs. 1 and 11.

In this study we use pseudopotentials to describe the atomic cores. This prevents us from actually promoting an electron to the conduction band from the core region and we have to resort to approximating the process. In order to get a broader picture of the theoretical consistency of core-level-energy calculations with pseudopotential methods for this material, we compare three different approximations. The methods are: the initial-state approximation, the excited-core approximation, and the $Z+1$ approximation, all of which will be briefly described in the following sections.

1. Initial-state approximation

The simplest approximation is to neglect final-state effects and use only the change in the initial-state energy part of Eq. (1) as the CLS. The initial-state approximation hence neglects the relaxation of the valence charge density in response to the ejection of the core electron. The way the initial-state energy is approximated in our case is by the variation in the average local potential energy.[12] The idea is that the main change to the energy level of the core electron comes from the average change in the local potential. This approximation of the initial-state energy thus neglects fluctuations in the shape of the atomic potentials and the effect on the different electron levels by these fluctuations.

2. Excited-core approximation

In this approximation, the excited atom is represented by a new pseudopotential[13] that has a missing core electron. In this work, as we study the CLS of Te, we replace a Te atom at a particular site by an atom described by this new pseudopotential (Te^*) and calculate the binding-energy difference

$$\Delta E_B = E(\text{CdTe}_{1-y}\text{Te}_y^*\text{O}_x) - E(\text{CdTeO}_x), \tag{3}$$

where $E(\text{CdTe}_{1-y}\text{Te}_y^*\text{O}_x)$ is the total energy of the supercell with concentration of core-ionized atoms y equal to one over the number of Te atoms in the supercell. Substitution of Te by Te^* at different sites provides the site-dependent CLS.

3. Z+1 approximation

A simplified version of the excited-core approximation is the equivalent core approximation or $Z+1$ approximation.[14] This model is good when the spatial extension of the core-hole wave function is small compared to the valence orbitals. Then, the excited core can be represented by the addition of a proton to the nucleus, i.e., the next element of the periodic table. Hence, the CLS in the $Z+1$ approximation can be obtained calculating total energies of a supercell, replacing the excited atom in different sites by a pseudopotential of the next element of the periodic table (with atomic number $Z+1$). In our case this means that the Te^* atom is replaced by an iodine atom in Eq. (3).

B. Calculation method

The first principles, self-consistent electronic-structure calculations were performed by means of DFT (Refs. 8 and 9) using two methods: the projected augmented wave method[15] as implemented in the Vienna *ab initio* simulation package (VASP),[16] and the pseudopotential method implemented in QUANTUM ESPRESSO (Q-E) (Ref. 17) code. The exchange-correlation energy (for all cases) was calculated using the generalized gradient approximation with the Perdew, Burke, and Ernzerhof functional.[18]

The electronic states in the DFT calculation were expanded using a plane-waves-basis set with cutoff of 400 eV. We used the projected augmented wave potentials with the valence states $5s$ and $5p$ for Te, $4d$ and $5s$ for Cd and $2s$ and $2p$ for O. The number of k points was carefully optimized in order to achieve energy convergence. Hence, the Brillouin zone was sampled using a $2\times2\times2$ Monkhorst-Pack. In the QUANTUM ESPRESSO calculations we employed the same parameters but cutoffs of 530 and 3264 eV for the wave functions and the charge density, respectively.

We used the pseudopotential generator included in QUANTUM ESPRESSO to generate the excited-core pseudopotential for Te by means of a scalar-relativistic calculation. The core excitation consisted in a hole in the $3d$ orbital. The cutoff radius for $5s$, $5p$, and $5d$ valence orbitals were chosen, respectively, at 2.1, 2.4, and 2.4 atomic units. The Rappe-Rabe-Kaxiras-Joannopoulus pseudization[11] was used in the generation procedure.

In the present investigation, we utilized structural models for amorphous $CdTeO_x$ obtained by MD simulations and previously published in Ref. 10 [structures can be found in supplementary material (Ref. 19)]. The supercell sizes for $CdTeO_x$ were adjusted by linear interpolation to fit the experimental densities of the crystalline materials CdTe [$\rho(\text{CdTe})=5.85\ \text{g/cm}^3$] and $CdTeO_3$ [$\rho(\text{CdTeO}_3)=6.416\ \text{g/cm}^3$]. The total number of atoms in each supercell was 66, 72, 76, and 80 for $x=0.2$, 1, 2, and 3, respectively. These numbers appear to be appropriate to describe these amorphous oxides as can be seen in the analysis of the pair-distribution functions, angle-distribution functions, and coordination histograms in Ref. 10.

To arrive at an amorphous structure the following steps were taken: the starting configuration had the atoms located at random nonoverlapping positions. The second step was to run the MD simulation, using the Verlet algorithm, with velocity rescaling at every step to keep the temperature fixed at 3000 K. A first run with a volume 50% higher than the experimental one was made during 0.5 ps, in order to facilitate ion diffusion from the initial configuration. The MD simulation was continued with the physical volume for 3–5 ps, depending on the oxygen content. Third, a velocity rescaling was performed using the Berendsen algorithm to drive the system toward 300 K as slowly as possible.

In that study it was found that the CdTeO and $CdTeO_2$ compounds present more chemical and topological disorder than $CdTeO_{0.2}$ and $CdTeO_3$.

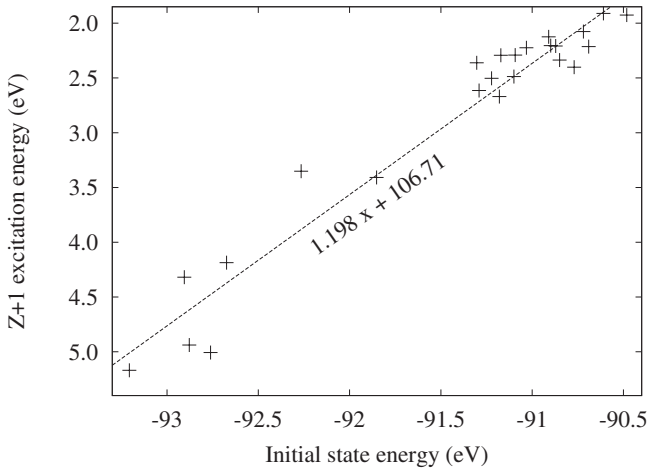

FIG. 1. Correlation between the initial-state approximation and $Z+1$ excitation energy for CdTeO. The other compounds studied here also exhibit the same behavior.

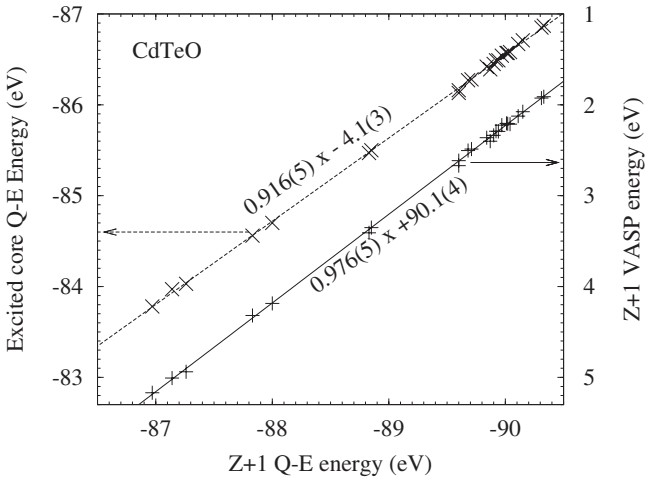

FIG. 2. (Right y axis) Comparison between the CLS calculated by VASP and Q-E in the $Z+1$ approximation. (Left y axis) Comparison of CLS calculated with Q-E within the excited-core approximation and the $Z+1$ approximation.

III. RESULTS AND DISCUSSION

A. Comparison of methods

In this section we compare the calculated CLS for CdTeO using the three approximations described above: the initial-state approximation, the $Z+1$ approximation, and the excited-core approximation. The $Z+1$ excitation energy and the average potential energy for Te atoms, calculated with VASP for CdTeO, are plotted in Fig. 1. In both approximations the CLS are grouped in two ranges that implies a two-peak structure of the spectrum. The approximations are well correlated and the other compounds in this study follow a similar behavior. The correlation coefficient close to 1 suggests that the initial-state approximation describes the main part of the mechanism behind the CLS for this material. Despite the fact that we observe this correlation, the scattering off the straight line suggests that it is important to include the final-state electron relaxation in the binding energy.

In Fig. 2 we also compare the $Z+1$ CLS in CdTeO, calculated with two *ab initio* codes, VASP (right y axis) and QUANTUM ESPRESSO. As can be seen, there is an almost perfect correlation between the CLS produced by the two codes. Let us note that the absolute values of the $Z+1$ energies are arbitrary as they contain a contribution from the pseudopotentials. The fact that different pseudopotentials are used by VASP and Q-E highlights the robustness of the $Z+1$ approximation. We also show in Fig. 2 a comparison between the CLS in CdTeO calculated by QUANTUM ESPRESSO using the excited core (left y axis) and the $Z+1$ approximation. Here we observe as well an excellent correlation between the $Z+1$ and the excited-core approximations, which, in addition to the discussion above, suggests good consistency and robustness of our method. In the following, we will only show results obtained by the $Z+1$ method.

B. Local-environment effects in spectral peaks

Figure 3 displays the calculated tellurium XPS spectra as calculated by means of the $Z+1$ approximation in VASP where the CLS of each local Te environment is shown by vertical bars. The height of each bar represents the number of oxygen neighbors of the particular Te site. In counting the number of oxygen neighbors we employed a radial cutoff of 2.32 Å, which is the distance of the first minimum of the partial Te-O radial distribution function of our structures.[10] To compute the spectrum, the calculated electron-core-level energies were represented by normalized Gaussians of width 0.5 eV which then were summed up to form the continuous line of the spectrum. The amount of broadening is always somewhat arbitrary but our choice was based on the ~0.2 eV resolution in the experiment described in Ref. 3 and the fact that the calculation represents a low sampling of the total amount of local environments which may be partially corrected by making the broadening a little larger.

We observe in Fig. 3 that each peak has associated tellurium atoms with different local environments. Thus, each

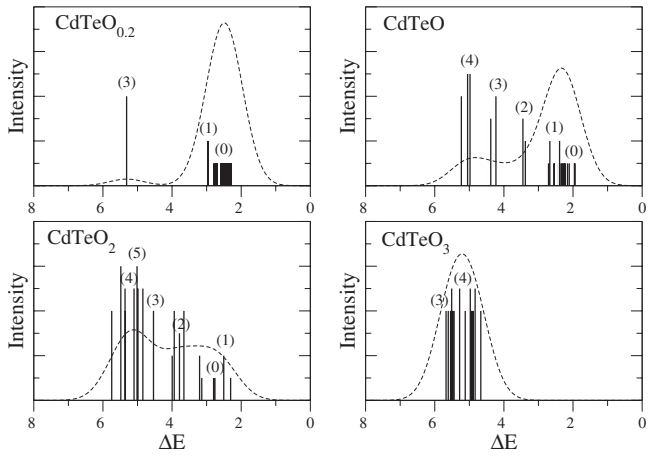

FIG. 3. The calculated tellurium XPS spectra are shown for $CdTeO_{0.2}$, CdTeO, $CdTeO_2$, and $CdTeO_3$. The bars indicate the tellurium energy shifts. The height of the bars and the numbers in parenthesis denote the number of oxygen neighbors, which was calculated within a cut-off radius of 2.32 Å.

peak contains contributions from one or more tellurium with a different number of oxygen neighbors. In particular, we can see that the peak on the right-hand side is coming mainly from Te atoms with 0 and 1 oxygen nearest neighbor and the peak on the left-hand side mainly by Te atoms with three to five oxygen neighbors. The Te atoms that have two oxygen neighbors tend to experience varying core-level shifts and cannot be assigned to any of the two spectral peaks. In general, the trend is that the binding energy increases as a function of oxygen atoms around Te but the conclusion must be that both peaks contain a signal from Te atoms with at least one oxygen atom in the local environment.

A well-established interpretation of the initial-state shift is that it captures the effects on the CLS from changes in the on-site local potential.[20,21] In this case we believe that the main effect on the local potential is due to interatomic charge redistributions. That means, however, that if final-state effects such as screening of the core hole are important, the initial-state shift may be a very poor approximation of the CLS. On the other hand, since the initial-state shift describes the CLS well in our case we must conclude that charge redistribution is the main effect on the CLS. Since our initial state shift is well correlated with the $Z+1$ approximation, our interpretation is that a large part of the CLS depends on the amount of charge redistributed from the Te site and that this in turn depends on the amount of oxygen in the neighborhood.

Hence, our interpretation of Fig. 3 is that one, and in some cases even two oxygen neighbors do not redistribute enough charge to place a particular Te shift in the left peak of the XPS spectrum. What determines the ambiguity for the two-correlated Te atoms is a subtle matter that deserves a focused study that is beyond our present possibilities.

When discussing these amorphous spectra in the literature, the peak on the right-hand side [cf. the peak at 582 eV in left panel of Fig. 4] has often been assigned to Te bound to Cd atoms while the left peak [cf. the peak at 585 eV in Fig. 4] has been assigned to Te bound to O,[3,5,7] however, the results in Fig. 3 clearly show that the interpretation of the peaks is more complex.

In Fig. 4 we compare the experimental (Ref. 3) (left side) and theoretical XPS spectra (right side) for CdTe oxide films. The Te $3d$ level is split due to relativistic effects and the XPS spectra show separate peaks for excitation of the Te $3d_{3/2}$ and Te $3d_{5/2}$ levels. Only the Te $3d_{3/2}$ peak is shown in Fig. 4 but the shape and trend of the Te $3d_{5/2}$ is the same, hence our calculation of the CLS applies to both peaks. The NH_3 partial-pressure values are given on top of each curve in the left panel in units of 10^{-4} Pa. This pressure is the experimental growth parameter that controls the amount of oxygen.

We find a qualitative agreement between some of the theoretical and experimental spectra where the theoretical $CdTeO_{0.2}$, CdTeO, $CdTeO_2$, and $CdTeO_3$ spectra and the experimental data corresponding to NH_3 partial pressures of 8, 11, 27, and 133×10^{-4} Pa, respectively, have quite similar peak structures. This concordance suggests that the computer-generated structures we are using to describe these amorphous materials indeed describe the experiments well. The distance between the peaks is however smaller in the calculated spectra by close to 1 eV. An error of this magnitude must be expected due to the problem of describing core-level relaxations with a pseudopotential as well as due to the well-known problem of describing the strong electron correlation in transition-metal oxides.

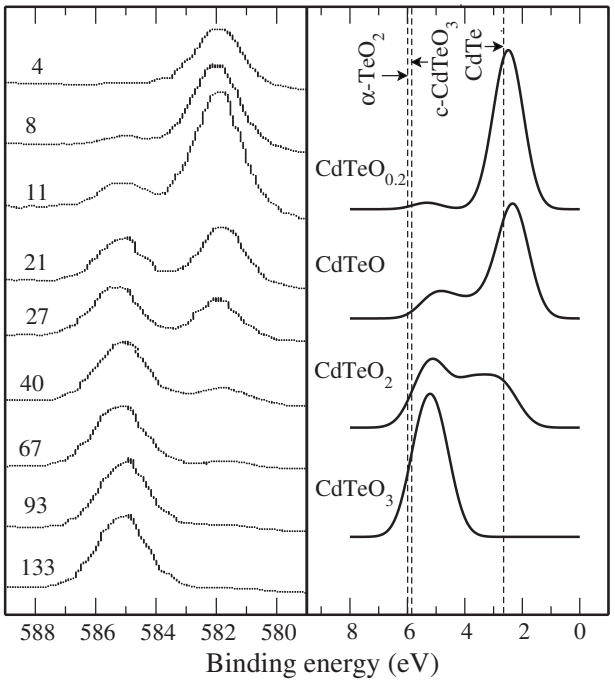

FIG. 4. In the left panel we show the experimental XPS data for the Te $3d_{3/2}$ peak reproduced from Ref. 3. The labels on the vertical axis correspond to relative NH_3 pressures for each experiment expressed in units of $\times10^{-4}$ Pa. In the right panel, we present the calculated spectra as obtained in the $(Z+1)$ approximation. The dashed vertical lines indicate core-level shifts for calculated α-TeO_2, c-$CdTeO_3$, and CdTe crystal structures. The binding-energy scale of the theoretical results is not absolute and only energy differences may be compared to experiments.

We indicate in Fig. 4 the calculated $Z+1$ Te binding energies of CdTe, α-TeO_2,[22] and c-$CdTeO_3$ (Ref. 23) crystals with vertical dashed lines, where Te atoms are strictly in Cd or O environments. In amorphous $CdTeO_x$, most Te atoms are bond to both Cd and O, as well as to Te.[10] This diversity of environments causes that the XPS peaks shift with respect to the pure Te-Cd and Te-O energies of the crystalline compounds.

C. Global composition

In the previous section we found that both Te peaks consist of signals from Te atoms with oxygen present in the local environment and that the calculated spectra are similar to some experimental results. From the comparison above we have still not made a quantitative comparison between the theoretical results and the experiments. To do so we investigate the relation between oxygen content and NH_3 partial pressure, a quantity that was experimentally determined in Ref. 3.

We make our quantification procedure as follows: by fitting each spectrum with two Gaussian functions we calculate

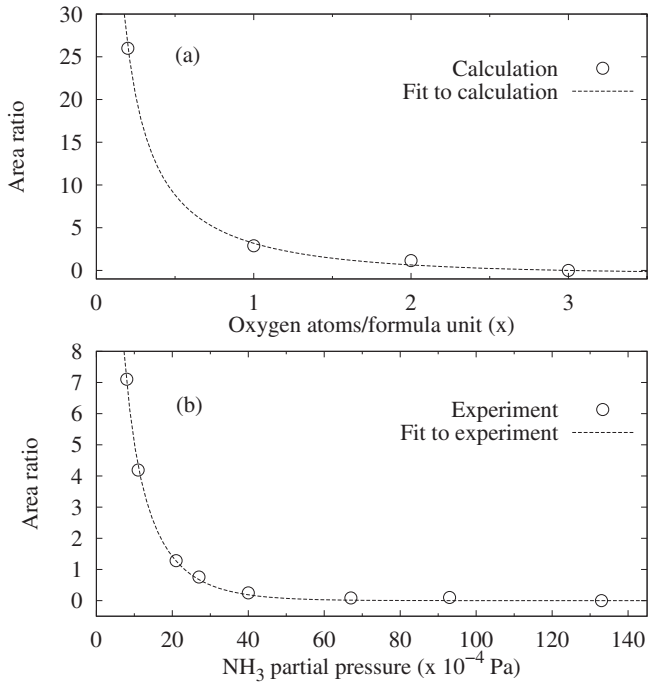

FIG. 5. The ratio between the Gaussian areas of each peak in the calculated tellurium XPS spectra is plotted in the upper graph as a function of the oxygen content x. The lower graph contains the same ratios as obtained from experiments (Ref. 3) but plotted as a function of NH_3 partial pressure. The dashed lines show the fits to the different data sets.

the ratio of the peak areas.[24] That provides a relation between the experimental peak-area ratios and NH_3 partial pressures as well as between theoretical peak-area ratios and oxygen content. Both relations are fitted with the function

$$y = a - \frac{b}{1 - e^{cx}}, \tag{4}$$

where y is the area ratio and x is either the oxygen content or the NH_3 partial pressure.[25] We display the calculated area ratios versus oxygen content and the experimental area ratios versus partial pressure in Fig. 5. In the fitting of the theoretical area ratio versus oxygen concentration the a parameter was set to $a=b/(1-e^{cx_{\max}})$ and $x_{\max}$ was chosen to be equal to 3.0. This constraint was included since the maximum oxygen content in our calculations is $x=3$, i.e., where the peak on the right-hand side in the $CdTeO_3$ spectrum disappears [cf. Figs. 3 and 4].

Now we can use the curves in Fig. 5 to find a one-to-one correspondence between the oxygen content and NH_3 partial pressure. Thus by combining both fits described above we obtain the following expression that relates oxygen content x and NH_3 partial pressure P:

$$x(P) = \frac{1}{c_t} \ln\left(1 - \frac{b_t(1 - e^{c_e P})}{b_e + (a_t - a_e)(1 - e^{c_e P})}\right), \tag{5}$$

where the indices t and e stand for theoretical and experimental fitting parameters, respectively. In Fig. 6 we plot the expression in Eq. (5) as a solid line and the experimental data from Ref. 3 as open pentagons. We observe that this expression reproduces quite well the experimentally determined oxygen contents at low pressures. For higher pressures though there is an offset so that in the asymptotic limit the experimental maximum oxygen content is $x=3.26$ while $x=3$ in the theoretical case. The theoretical asymptotic limit results from the fact that $x=3$ was our highest investigated oxygen concentration. The exact asymptotic limit is very challenging to find theoretically due to limited supercell sizes in the calculations. The problem is that the probability to find Te sites without oxygen neighbors becomes very low in the compounds with high oxygen concentrations. Hence, we would have to include a much larger number of atoms in the calculations which, unfortunately, would bring the computational cost beyond our reach.

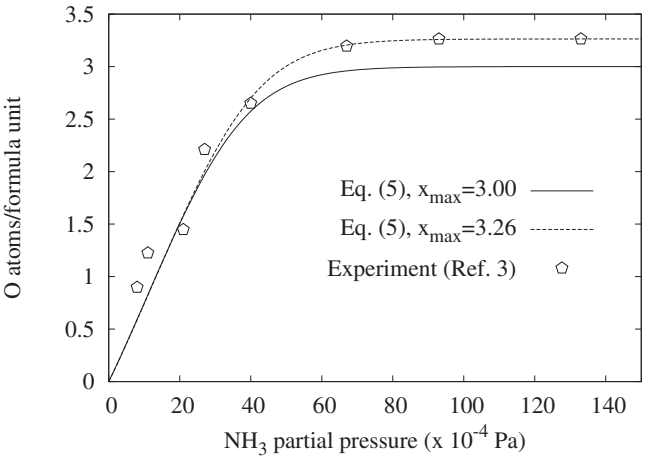

FIG. 6. The $x(P)$ expression obtained in Eq. (5) is displayed. The dashed curve is the corresponding refitted function with the experimental saturation limit. The open pentagons show the experimentally determined oxygen content from Ref. 3.

In order to correct for our lack of statistics in the high concentration limit, we may adjust the $x_{\max}$ parameter in the fit of the theoretical data to the experimental asymptotic value of $x=3.26$. The result is shown in Fig. 6 as a dashed curve.[26] The agreement between our calculation and the experimentally obtained relation between NH_3 partial pressure and oxygen content hence verifies that the amorphous structures used in the calculation describe the experimental situation well.

IV. SUMMARY

We have demonstrated excellent theoretical consistency between different first-principles DFT methods and approximations for calculating the site-specific core-level shifts in amorphous oxides. The effects of local Te environments on the XPS spectrum were calculated and it was shown that both peaks of the split Te $3d$ level contain contributions from Te with oxygen in the local environment, information that can only be obtained by combining first-principles calculations with experiments. From an analysis of the initial-state shifts, we conclude that the main effect on the core-level shift is due to interatomic charge redistributions. Our amor-

phous structures were shown to describe the global oxygen content well by comparing the area ratios of the two Te 3*d* peaks obtained from the calculations and the experiments. Our results show the importance of first-principles calculations when quantifying the details of XPS spectra in amorphous oxides, in particular, and complex materials, in general. We believe that this is an important result that will guide future characterizations of technologically important materials.

ACKNOWLEDGMENTS

This work was supported by the Anillo ACT/ADI-24 Chile grant and CONICYT under Grant No. ACI52. A.A. was supported by DID (UACH) under Grant No. S-2008-42. E.H. and R.L. also acknowledge support from FONDECYT under Projects No. 11070115 and No. 11080259 as well as DID (UACH) under Grants No. SR-2008-0 and No. S-2008-51. P.B. was supported by CONACYT under Grant No. 59998.

[1] *Core Level Spectroscopy of Solids*, edited by F. de Groot and A. Kotani (CRC, London, 2008), Vol. 6.
[2] E. Holmström, W. Olovsson, I. Abrikosov, A. Niklasson, B. Johansson, M. Gorgoi, O. Karis, S. Svensson, F. Schäfers, W. Braun, G. Öhrwall, G. Andersson, M. Marcellini, and W. Eberhardt, Phys. Rev. Lett. **97**, 266106 (2006).
[3] P. Bartolo-Pérez, R. C. Rodríguez, F. Caballero-Briones, W. Cauich, J. L. Peña, and M. H. Farias, Surf. Coat. Technol. **155**, 16 (2002).
[4] P. Bartolo-Pérez, J. L. Peña, and M. H. Farias, Superficies y Vacio **8**, 59 (1999).
[5] A. Zapata-Navarro, M. Zapata-Torres, V. Sosa, P. Bartolo-Pérez, and J. L. Peña, J. Vac. Sci. Technol. A **12**, 714 (1994).
[6] P. Bartolo-Pérez, J. Ceh, J. L. Peña, A. Zapata-Navarro, and M. H. Farias, Superficies y Vacio **15**, 30 (2002).
[7] M. Y. El Azhari, M. Azizan, A. Bennouna, A. Outzourhit, E. L. Ameziane, and M. Brunel, Thin Solid Films **295**, 131 (1997).
[8] P. Hohenberg and W. Kohn, Phys. Rev. **136**, B864 (1964).
[9] W. Kohn and L. Sham, Phys. Rev. **140**, A1133 (1965).
[10] E. Menéndez-Proupin, P. Giannozzi, J. Peralta, and G. Gutiérrez, Phys. Rev. B **79**, 014205 (2009).
[11] S. Hüfner, *Photoelectron Spectroscopy: Principles and Applications*, 2nd ed. (Springer, Berlin, 1995).
[12] M. P. J. Punkkinen, P. Laukkanen, K. Kokko, M. Ropo, M. Ahola-Tuomi, I. J. Väyrynen, H.-P. Komsa, T. T. Rantala, M. Pessa, M. Kuzmin, L. Vitos, J. Kollár, and B. Johansson, Phys. Rev. B **76**, 115334 (2007).
[13] E. Pehlke and M. Scheffler, Phys. Rev. Lett. **71**, 2338 (1993).
[14] B. Johansson and N. Maartensson, Phys. Rev. B **21**, 4427 (1980).
[15] P. E. Blöchl, Phys. Rev. B **50**, 17953 (1994).
[16] G. Kresse and J. Furthmüller, Phys. Rev. B **54**, 11169 (1996).
[17] P. Giannozzi, S. Baroni, N. Bonini, M. Calandra, R. Car, C. Cavazzoni, D. Ceresoli, G. L. Chiarotti, M. Cococcioni, I. Dabo *et al.*, J. Phys.: Condens. Matter **21**, 395502 (2009).
[18] J. P. Perdew, K. Burke, and M. Ernzerhof, Phys. Rev. Lett. **77**, 3865 (1996).
[19] See supplementary material at http://link.aps.org/supplemental/10.1103/PhysRevB.79.014205 for the atomic coordinates in XYZ format.
[20] I. A. Abrikosov, W. Olovsson, and B. Johansson, Phys. Rev. Lett. **87**, 176403 (2001).
[21] G. K. Wertheim, R. L. Cohen, G. Crecelius, K. W. West, and J. H. Wernick, Phys. Rev. B **20**, 860 (1979).
[22] P. A. Thomas, J. Phys. C **21**, 4611 (1988).
[23] V. Krämer and G. Brandt, Acta Crystallogr., Sect. C: Cryst. Struct. Commun. **41**, 1152 (1985).
[24] There are several ways to subtract the background in the experimental data and each method have some uncertainty. In our case we chose to approximate the background as a straight line.
[25] The fitting parameters to the experimental data are $a=0$, $b=7.87$, and $c=0.094$. The theoretical fitting parameters are $a=0.35$, $b=5.53$, and $c=0.94$.
[26] The new fit for the theoretical relation of area ratio against oxygen concentration, which considers the experimental limit of oxygen concentration resulted in the following fitting parameters: $a=0.23$, $b=5.80$, and $c=0.998$.